

5 Mohamad Behjati Ashtiani<sup>1</sup>, Mohammadhossein Akhavanfar<sup>2</sup>, Lingyu Li<sup>1</sup>, Sunwook Kim<sup>1</sup>,  
6 Maury A. Nussbaum<sup>1</sup>

<sup>7</sup> <sup>1</sup>Department of Industrial and Systems Engineering, Virginia Tech, Blacksburg, VA, USA

<sup>8</sup> <sup>2</sup>School of Human Kinetics, Faculty of Health Sciences, University of Ottawa, Ottawa, Ontario, K1N  
<sup>9</sup> 6N5, Canada

10 Mohamad Behjati Ashtiani, Msc. (mohamadbehjati@vt.edu)  
11 Mohammadhossein Akhavanfar, Ph.D. (makha037@uottawa.ca)  
12 Lingyu Li, BSc. (lingyu99@vt.edu)  
13 Sunwook Kim, Ph.D. (sunwook@vt.edu)

## **15 \*Corresponding Author:**

16 Maury A Nussbaum, PhD, Virginia Tech  
17 Blacksburg, Virginia, United States.  
18 Email: [nussbaum@vt.edu](mailto:nussbaum@vt.edu)  
19 Phone: (540) 231-6053  
20 Word count (from “Introduction” through “conclusion”): **3466**, Word count (abstract): **229**

22   **Abstract**

23   Occupational back-support exoskeletons (BSEs) can reduce physical demands during lifting by providing  
24   assistive torques, but their effects on spine loading are poorly understood. In this study, we used two  
25   common musculoskeletal models developed in OpenSim and the AnyBody Modeling System to estimate  
26   intervertebral joint forces (IJF) during asymmetric and symmetric lifting tasks with and without BSEs.  
27   Data from an earlier study were used, involving 18 participants who performed repetitive lifting/lower in  
28   three task conditions and with three different BSEs (along with a control condition using no BSE). We  
29   simulated the tasks with both models and estimated axial compression and anteroposterior shear forces at  
30   the L4/L5 joint and derived peak values (95<sup>th</sup> percentile) as outcome measures. OpenSim estimated  
31   significantly larger axial compression and anteroposterior shear forces than AMS. Both models estimated  
32   reductions in spine loading when using either of the BSEs, though OpenSim estimated greater reductions  
33   than AMS. Strong positive, linear relationships ( $r > 0.95$ ) between the two model estimates were found for  
34   axial compression, while much weaker and even negative relationships were observed for shear forces,  
35   especially under asymmetric conditions. The differences in model estimates were likely due to variations  
36   in model assumptions and passive tissue representations. Future research should explore more detailed  
37   human-exoskeleton interaction models, evaluate the impact of modeling assumptions on IJF estimates,  
38   and assess the agreement of these findings with *in vivo* measurements such as electromyography.

39

40   **Keywords:**

41   Back-Support Exoskeletons, Musculoskeletal Modeling, AnyBody Modeling System, OpenSim, Spine

1

2

Original Article

# Using musculoskeletal models to estimate the effects of exoskeletons on spine loads during dynamic lifting tasks: differences between OpenSim and the AnyBody Modeling System

6

7 Mohamad Behjati Ashtiani<sup>1</sup>, Mohammadhossein Akhavanfar<sup>2</sup>, Lingyu Li<sup>1</sup>, Sunwook Kim<sup>1</sup>, Maury A  
8 Nussbaum<sup>1</sup>

<sup>9</sup> <sup>1</sup>Department of Industrial and Systems Engineering, Virginia Tech, Blacksburg, VA, USA

**12** Word count (from “Introduction” through “conclusion”): **3466**

**\*Corresponding Author:**

14 Maury A Nussbaum, PhD, Virginia Tech

15 Blacksburg, Virginia, United States.

16 Email: nussbaum@vt.edu

17 Phone: (540) 231-6053

18

19    **Abstract**

20    Occupational back-support exoskeletons (BSEs) can reduce physical demands during lifting by providing  
21    assistive torques, but their effects on spine loading are poorly understood. In this study, we used two  
22    common musculoskeletal models developed in OpenSim and the AnyBody Modeling System to estimate  
23    intervertebral joint forces (IJF) during asymmetric and symmetric lifting tasks with and without BSEs.  
24    Data from an earlier study were used, involving 18 participants who performed repetitive lifting/lower in  
25    three task conditions and with three different BSEs (along with a control condition using no BSE). We  
26    simulated the tasks with both models and estimated axial compression and anteroposterior shear forces at  
27    the L4/L5 joint and derived peak values (95<sup>th</sup> percentile) as outcome measures. OpenSim estimated  
28    significantly larger axial compression and anteroposterior shear forces than AMS. Both models estimated  
29    reductions in spine loading when using either of the BSEs, though OpenSim estimated greater reductions  
30    than AMS. Strong positive, linear relationships ( $r > 0.95$ ) between the two model estimates were found for  
31    axial compression, while much weaker and even negative relationships were observed for shear forces,  
32    especially under asymmetric conditions. The differences in model estimates were likely due to variations  
33    in model assumptions and passive tissue representations. Future research should explore more detailed  
34    human-exoskeleton interaction models, evaluate the impact of modeling assumptions on IJF estimates,  
35    and assess the agreement of these findings with *in vivo* measurements such as electromyography.

36

37    **Keywords:**

38    Back-Support Exoskeletons, Musculoskeletal Modeling, AnyBody Modeling System, OpenSim, Spine

39 **1. Introduction**

40 Occupational back-support exoskeletons (BSEs) have emerged as an ergonomic intervention that can  
41 reduce physical demands on the back during work tasks and thereby potentially reduce the risk of work-  
42 related musculoskeletal disorders (de Looze et al., 2016; Kazerooni, 2008; Lee et al., 2012). In particular,  
43 BSEs can reduce muscle activity, perceived exertion, and energy expenditure during various manual  
44 tasks, including symmetric and asymmetric lifting and prolonged trunk bending (Ali et al., 2021;  
45 Kermavnar et al., 2021). The beneficial (and undesirable) effects of BSE use can also depend on various  
46 factors including the performed task, BSE design, and individual characteristics such as biological sex  
47 (e.g., Alemi et al., 2020; Bosch et al., 2016; Lamers et al., 2017; Madinei et al., 2020). Yet, it remains  
48 generally unclear whether BSEs can effectively reduce spine loading, although such loading is a common  
49 direct indicator of low back disorder risk (Waters et al., 1993). This uncertainty arises from the wearable  
50 nature of BSEs, which complicates estimating spine loading using detailed musculoskeletal models. For  
51 example, it is difficult to use models based on surface electromyography (EMG), due to challenges in  
52 electrode placement and signal quality while wearing a BSE. While some researchers have used such  
53 models to estimate spine loading (Eskandari et al., 2025; Koopman, Kingma, et al., 2020; Koopman, Näf,  
54 et al., 2020), the study protocols were limited to short durations and simple lifting tasks.

55

56 Musculoskeletal modeling tools, such as the widely used AnyBody Modeling System™ (AMS;  
57 Damsgaard et al., 2006) and OpenSim (Delp et al., 2007), have been a basis to virtually design BSEs  
58 while accounting for human-exoskeleton interactions (Chander et al., 2022; Ma et al., 2023). Investigators  
59 have also used these tools to estimate the effects of BSEs on wearers, finding that BSE use can  
60 significantly reduce physical demands, including estimated joint reaction forces and muscle activations  
61 (Banks et al., 2024; Madinei & Nussbaum, 2023; Schmalz et al., 2022; Yan et al., 2024). However, there  
62 are no reports, to our knowledge, regarding whether different musculoskeletal modeling tools produce  
63 consistent estimates of spine loading in dynamic lifting tasks, especially in the context of BSE use.  
64 Potential inconsistencies could arise from variations in simulation packages and the differing assumptions

65 underlying the musculoskeletal models within these tools (Ghezelbash et al., 2020; Kim et al., 2018). We  
66 believe that identifying potential inconsistencies will help in using these models to guide BSE design and  
67 to evaluate BSE biomechanical effects in diverse applications.

68

69 In the current study, we compared spine loads estimated from AMS and OpenSim during symmetric and  
70 asymmetric lifting and lowering tasks, when both tasks were done with and without two distinct BSEs.  
71 This work represents an initial effort to explore the application of these modeling tools in assessing BSE  
72 benefits and limitations. Our objective was not to validate modeling outcomes (e.g., against a “gold  
73 standard”), but rather to examine the consistency (or inconsistency) of their outputs across different task  
74 conditions. To maintain a practical (user-centered) perspective, we compared current versions of the  
75 available musculoskeletal models without harmonizing modeling approaches or detailed specifications.  
76 Given existing differences in modeling principles and assumptions, we hypothesized that these tools  
77 would estimate *quantitatively different* spine loads during BSE use. Nonetheless, based on previous  
78 findings on the effects of BSEs on spine loading, we also hypothesized that both tools would yield  
79 *qualitatively similar* estimates of such BSE effects.

80

## 81 **2. Materials and methods**

### 82 **2.1 Experimental setup and data pre-processing**

83 Data used here were obtained in a previously reported study (Madinei et al., 2020), the details of which  
84 are only summarized here. Eighteen participants (9 females, 9 males) performed trials involving repetitive  
85 lifting/lowering in each of nine conditions ( $3 \text{ Task Conditions} \times 3 \text{ Interventions}$ ). The *Task Conditions*  
86 were: symmetric lifting/lowering to/from mid-shank height (Ground\_Sym) and to/from knee height  
87 (Knee\_Sym), and asymmetric lifting/lowering to/from knee height at a 90° asymmetry angle (Knee\_Asy).  
88 The *Intervention* levels included two BSEs (suitX backX™ AC and Laevo™ V2.5) and a control  
89 condition (no BSE). Each trial comprised 40 cycles of freestyle lifting/lowering a box (set to 10% of  
90 individual body mass) at a rate of 10 cycles per minute over a 4-min. duration. Whole-body kinematics

were recorded at 60 Hz using an inertial motion capture system (MVN Awinda, Xsens Technologies, Netherlands). Kinematic data were saved in BioVision Hierarchy (BVH) files, using the International Society of Biomechanics recommended ZXY intrinsic rotation sequence (Wu et al., 2005) and subsequently filtered using a second-order, zero-lag, low-pass Butterworth filter (5 Hz cut-off frequency).

95

## 96 **2.2 Musculoskeletal models**

We used the generic gait-full-body model from the AnyBody™ Managed Modeling Repository (v3.0.1) in AMS. Earlier work showed that this model generated estimates of L4/L5 spine loads that had a strong positive correlation with *in vivo* measurements during dynamic lifting tasks (Bassani et al., 2017). In OpenSim (v4.5), we used the enhanced, fully articulated thoracolumbar spine (FATLS) full-body generic model that was developed by Akhavanfar et al. (2024). Building on the spine model introduced by Bruno et al. (2015), the enhanced FATLS incorporates passive intervertebral stiffness and was demonstrated to estimate resultant L1/L2 spine loads that had a strong positive correlation with direct measurements of vertebral implant forces during dynamic lifting tasks. Also, the original FATLS vertebral compressive loading estimates, including spine loads from the lumbar and thoracic regions of the model (including at L4/L5), were strongly correlated with intradiscal pressure measurements for a variety of symmetric and asymmetric activities (Bruno et al., 2015). Table A1 (see Supplemental Material) provides additional detailed information on the models we used within AMS and OpenSim.

109

## 110 **2.3 Lifting and lowering simulation and modeling**

AMS and OpenSim estimate muscle activation levels and forces via processes that include: 1) scaling the generic model to match individual anthropometric dimensions and adjusting muscle moment arms and cross-sectional areas; 2) performing an inverse kinematic analysis to obtain joint kinematics; 3) completing an inverse dynamics analysis to obtain the net forces and moments at all joints; and 4) estimating muscle forces by solving a static optimization problem. OpenSim can also include a residual reduction algorithm before the final step, however we excluded this algorithm since we did not have force

plate data. Simulations for each experimental trial were performed separately for each lifting and lowering phase using both AMS and OpenSim. In these simulations, we assumed the box mass to be evenly distributed between the hands (we did not have hand force data). For each participant and experimental condition, intervertebral joint forces (IJFs) were computed at the L4/L5 level. We focused on this level since earlier studies also compared model estimates here vs. *in vivo* measurements (Bassani et al., 2017; Bruno et al., 2015).

123

#### 124 *Implementing the AnyBody Modeling System (AMS)*

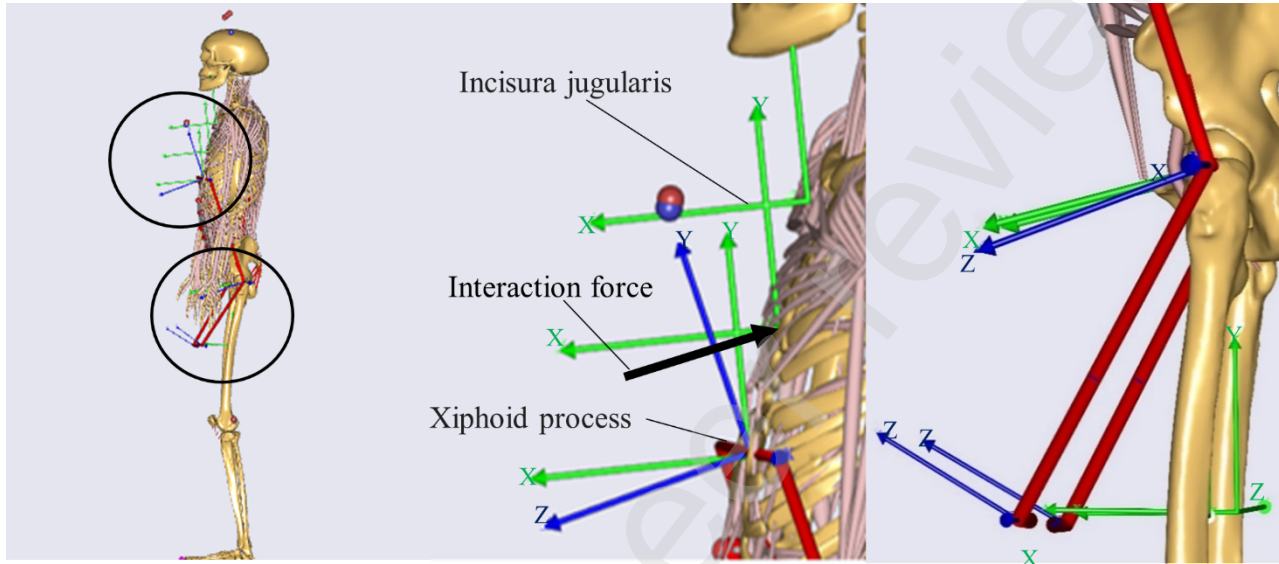
125 Using AMS built-in routines, the Gait-full-body model was first scaled to each participant based on  
126 segment lengths derived from the BVH files (Karatsidis et al., 2019). This scaling specifically adjusted  
127 body segment geometry, mass, inertial properties, and maximum isometric muscle forces (Rasmussen et  
128 al., 2005). Inverse kinematics was performed by aligning virtual marker (VM) locations on human models  
129 to corresponding VMs from the built-in stick figure model generated from BVH files, using a kinematic  
130 optimization that minimized weighted least-squares differences between the VM positions on the stick  
131 figure and human model (Andersen et al., 2009). Muscle forces were computed through static  
132 optimization, minimizing the sum-of-squared normalized muscle forces while satisfying constraints on  
133 equilibrium and the non-negativity of muscle forces (Damsgaard et al., 2006).

134

135 To simulate a BSE, we created a virtual representation following the approach outlined by Madinei and  
136 Nussbaum (2023). The virtual BSE consisted of three massless dummy segments—a torso and two leg  
137 frames—connected via revolute joints. These segments were constrained to the Gait-full-body model at  
138 the hip joint and chest, allowing the torso frame to follow the trunk movement (Figure 1). Real-time  
139 support torques generated by each BSE were determined using the angle between these frames and  
140 torque-angle data we obtained from the manufacturers (in contrast to Madinei & Nussbaum, 2023, who  
141 used their own experimental measures). From the torque and moment arm (the length of the BSE torso  
142 frame), we estimated interaction forces between the torso segment and the chest of the Gait-full-body

143 model. These forces were applied to the thorax at a defined contact point located midway between the  
 144 incisura jugularis and xiphoid process (Figure 1), similar to Eskandari et al. (2025); this contact point  
 145 remained constant throughout the simulations.

146



147  
 148 Figure 1. Illustrations of a virtual BSE representation in the AnyBody Modeling System (AMS). The  
 149 middle and right figures show zoomed-in views of the coordinate systems for the BSE (blue) and the  
 150 Gait-full-body model (green) at the torso and leg frames, respectively. The black arrow indicates the  
 151 interaction force between the BSE and the Gait-full-body model, applied to a contact point on the chest  
 152 (the origin of the body coordinate system in green) and aligned parallel to the normal axis (blue Z-axis) of  
 153 the BSE torso plate (chest pad).

154

#### 155 *Implementing OpenSim*

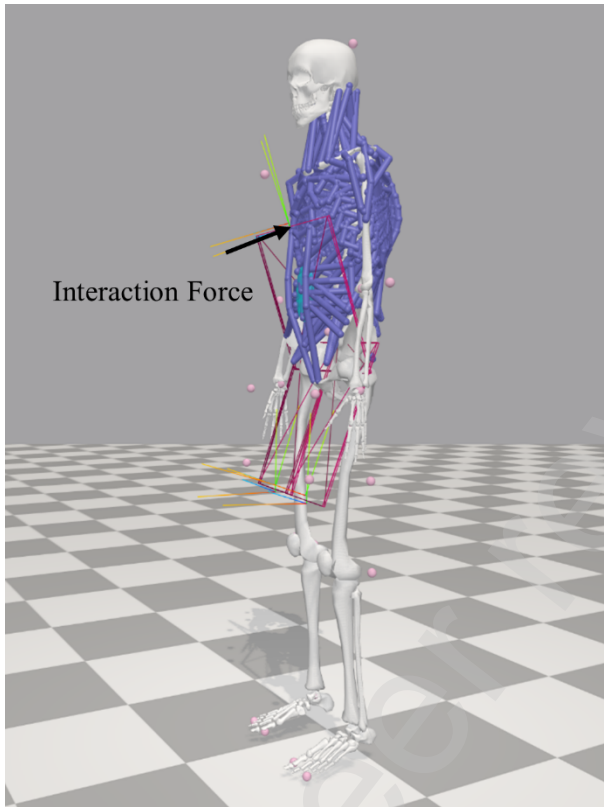
156 The FATLS model was scaled using the Scale Tool (Delp et al., 2007) based on VMs data from a static  
 157 N-pose (Wechsler et al., 2023) and using anthropometric data to adjust maximum isometric muscle forces  
 158 (Rasmussen et al., 2005). Marker data (.trc) for the VMs were extracted from the BVH files following the  
 159 method described by Wechsler et al. (2023). Inverse kinematics was performed using the Inverse  
 160 Kinematics Tool, which minimized weighted squared errors between the three-dimensional positions of

161 markers in the FATLS model and the corresponding VMs (Delp et al., 2007). Using the Static  
162 Optimization tool, inverse dynamics analysis was performed, followed by static optimization to minimize  
163 the sum of squared muscle activations while satisfying constraints on equilibrium and the non-negativity  
164 of muscle forces, while accounting for muscle force-length-velocity relationships.

165

166 A virtual BSE was added using a similar approach to AMS, comprising three dummy frames (BSE torso  
167 and two leg frames) interconnected via custom joints (see Figure 2). Interaction forces were calculated as  
168 in AMS and were applied to the thorax. But, the location of force application was defined in the local  
169 coordinate system of the BSE torso frame, which was positioned at the midpoint of the top BSE torso  
170 frame, parallel to the axis normal to the chest pad plate (Figure 2) rather than at the chest contact point as  
171 in AMS. This approach was used so that the application point of the interaction forces corresponded to the  
172 contact point of the BSE torso frame at the chest.

173



174  
175

Figure 2. Illustration of the virtual BSE representation in OpenSim. The black arrow represents the interaction force between the BSE and the FATLS model, which is applied to the thorax. Pink balls represent VMs in the human model.

179

180 2.4 Data processing and outcome measures

We ran 12,960 simulations, involving 18 participants  $\times$  9 trials  $\times$  40 cycles  $\times$  2 phases (lifting and lowering), in both AMS and OpenSim. Simulations were done using Python libraries—AnyPyTools for AMS (Lund et al., 2019) and the OpenSim API (v4.5). For each simulation, IJFs at the L4/L5 lumbar spine level were extracted and expressed in the L5 local coordinate system, specifically as axial compressive ( $F_C$ ) and anteroposterior shear ( $F_{AP}$ ) forces. Mediolateral shear forces were not analyzed since they were consistently of small magnitude (<100 N). We derived peak (95<sup>th</sup> percentile) values of  $F_C$  and  $F_{AP}$  as outcome measures within each lift/lower cycle. Peak values were of interest as they are common metrics for ergonomic assessments.

189

190 **2.5 Statistical Analyses:**

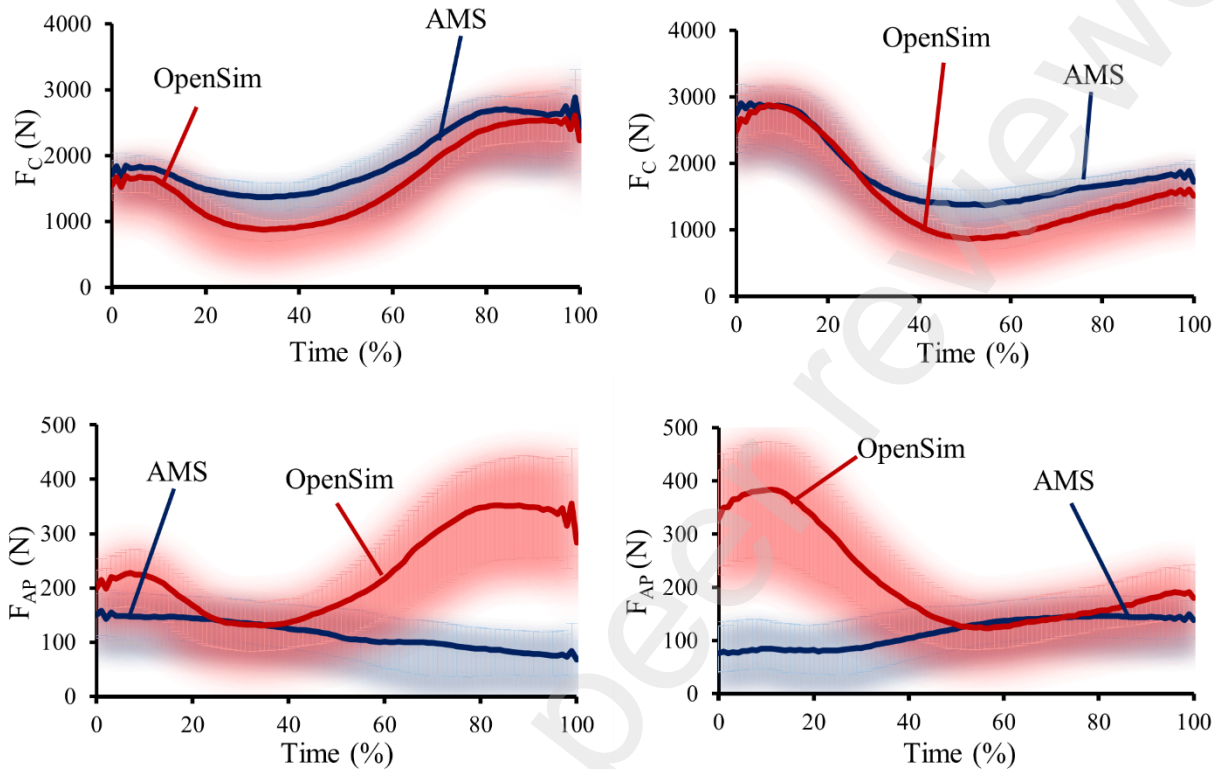
191 Repeated-measures analyses of variance (ANOVAs) were performed using JMP Pro 16 (SAS, Cary, NC)  
192 and applying the restricted maximum likelihood method. Four-way ANOVAs were used to assess the  
193 effects of *Task Condition*, *Intervention*, *Movement Phase*, and *Model* (i.e., AMS vs OpenSim) on peak  $F_C$   
194 and  $F_{AP}$ , with *Biological Sex* included as a blocking factor. Analyses were limited to three-way  
195 interactions to avoid practical difficulties in interpreting higher-order interactions. We also evaluated the  
196 linear association between estimates from the two models, by obtaining the Pearson Correlation  
197 Coefficient ( $r$ ) for each lifting/lowering cycle. We then used three-way ANOVAs to examine the effects  
198 of *Task Condition*, *Intervention*, and *Movement Phase* on the coefficients. In both sets of ANOVAs,  
199 lifting/lowering cycles were treated as replications, and the presentation orders of *Task Condition* and  
200 *Intervention* were included as blocking factors (*n.b.*, no significant order effects were found). Statistical  
201 significance was concluded when  $p < 0.05$ . To meet parametric model assumptions, all outcome measures  
202 except  $r$  for  $F_{AP}$  were log-transformed prior to analysis, with summary results back-transformed for  
203 presentation. A distinct transformation (Johnson Sb) was applied to the noted  $r$  values since there were  
204 negative values. Significant main and interaction effects were explored using *post hoc* paired comparisons  
205 (using Tukey's HSD) and simple effects tests, respectively. Given the study aims, the subsequent results  
206 presentation emphasizes effects involving *Intervention* and *Model*. Detailed ANOVA results are provided  
207 in Tables A2 and A3 in the Supplementary Material.

208

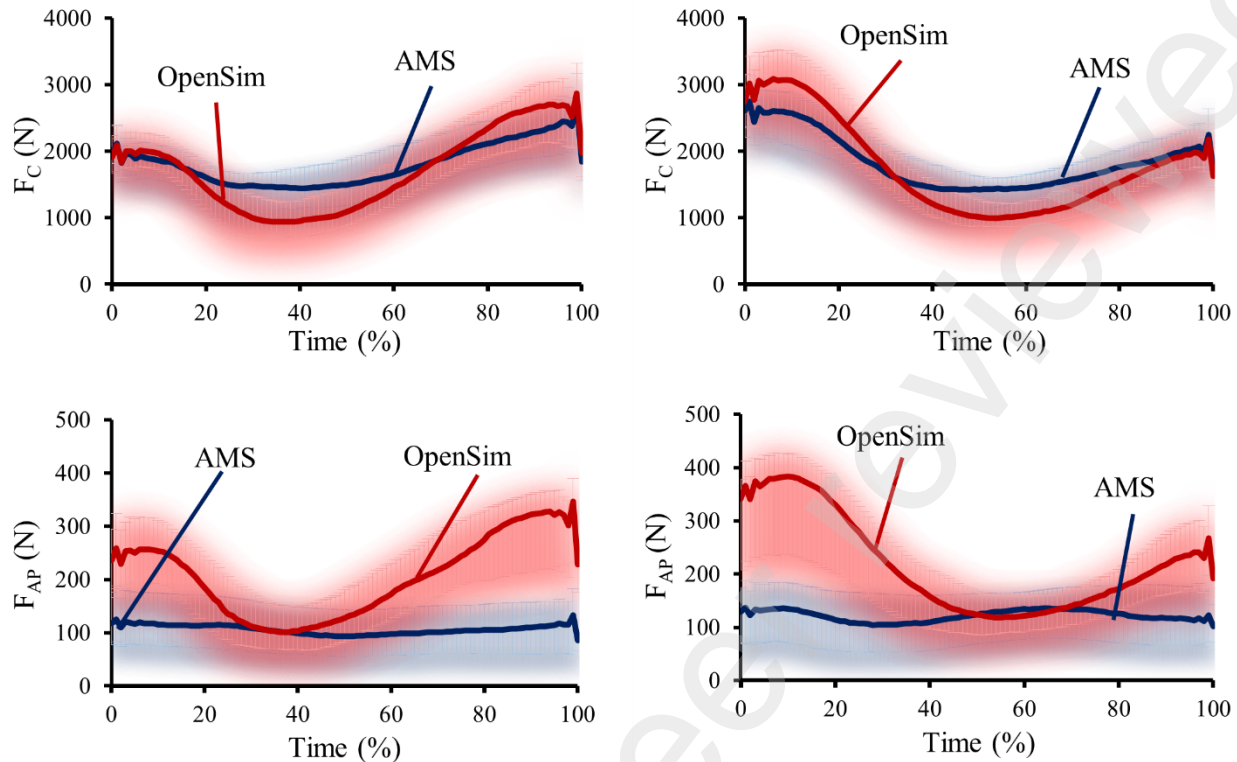
209 **3. Results**210 **3.1 Overall qualitative comparisons between AMS and OpenSim**

211 Model estimates of  $F_C$  had similar overall trends, yet OpenSim generally estimated larger values at the  
212 end of a lowering task or at the start of lifting, but lower values mid-task (Figures 3-4). Across the  
213 lifting/lowering tasks,  $F_{AP}$  forces estimated using OpenSim were consistently larger than those from AMS

214 (Figures 3-4). Additional ensemble plots are presented in Figures A1–A7 in the Supplementary Materials,  
 215 providing further comparisons between OpenSim and AMS.



216  
 217 Figure 3. Example ensemble median plots of intervertebral joint forces at the L4/L5 intervertebral joint,  
 218 comparing results from OpenSim and AnyBody (AMS) for the Knee\_Asy task when using backX. This  
 219 condition was selected as it represents the “worst” condition, highlighting substantial differences in  
 220 estimates of F<sub>AP</sub>. **Top left:** Compression Forces (F<sub>C</sub>) during lowering. **Top right:** F<sub>C</sub> during lifting.  
 221 **Bottom left:** Anteroposterior Shear Forces (F<sub>AP</sub>) during lowering. **Bottom right:** F<sub>AP</sub> during lifting.  
 222 Shaded areas represent 25<sup>th</sup> and 75<sup>th</sup> percentile values.  
 223



224  
 225 Figure 4. Example ensemble median plots of intervertebral joint forces at the L4/L5 intervertebral joint  
 226 comparing results from OpenSim and AnyBody (AMS) for the Knee\_Sym task when using Laevo. This  
 227 condition was selected as it represents the “best” condition, with similar trend for estimates of  $F_{AP}$ . **Top**  
 228 **left:** Compression Forces ( $F_C$ ) during lowering. **Top right:**  $F_C$  during lifting. **Bottom left:**  
 229 Anteroposterior Shear Forces ( $F_{AP}$ ) during lowering. **Bottom right:**  $F_{AP}$  during lifting. Shaded areas  
 230 represent the 25<sup>th</sup> and 75<sup>th</sup> percentile values.

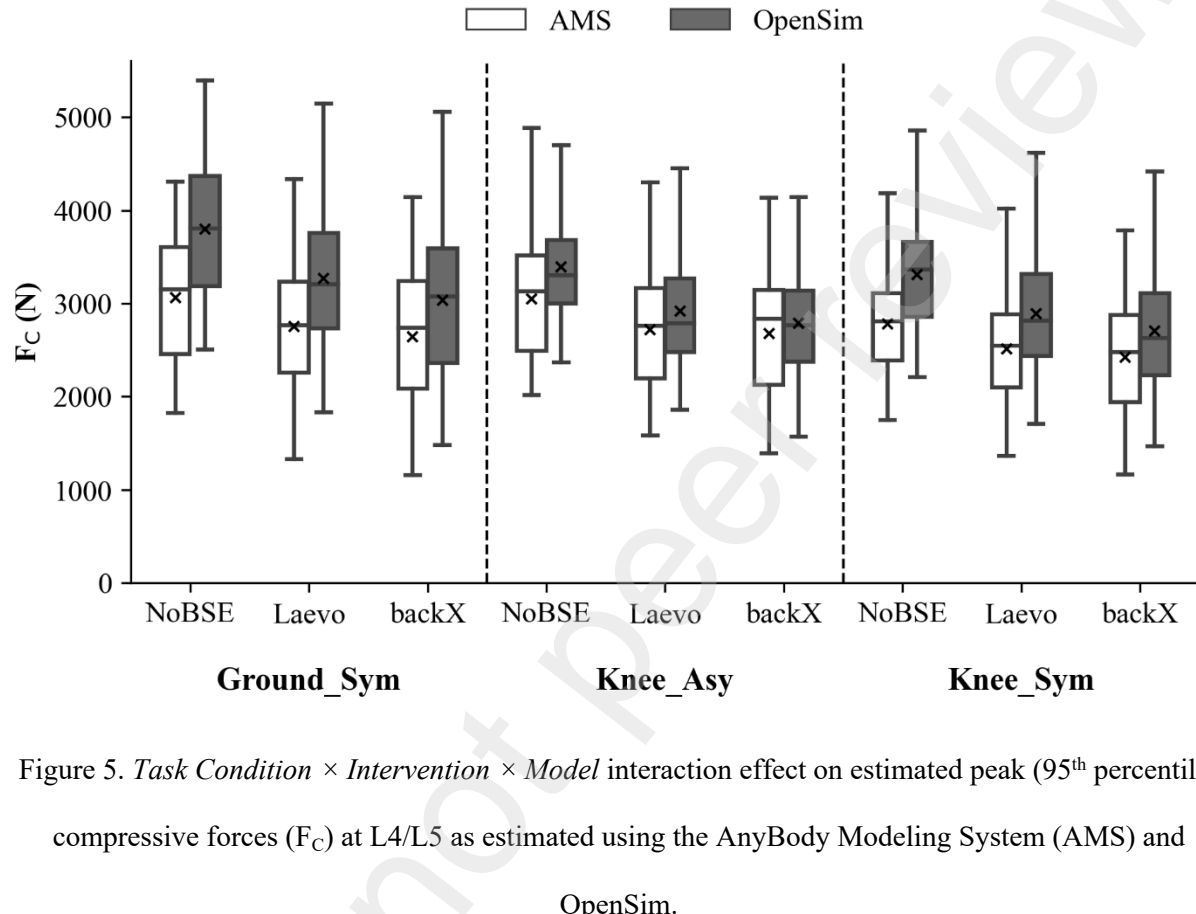
231

### 232 3.2 Peak compression force ( $F_C$ ) at L4/L5

233 The *Task Condition*  $\times$  *Intervention*  $\times$  *Model* interaction effect was significant on peak  $F_C$ . Simple effects  
 234 analysis indicated significant *Intervention*  $\times$  *Model* effects across all *Task Conditions*, as well as  
 235 significant *Task Condition*  $\times$  *Model* effects across all *Interventions*. Despite this complexity, there were  
 236 some consistent outcomes. Specifically, OpenSim estimated significantly larger (9-13%) peak  $F_C$  than  
 237 AMS across all conditions (Figure 5). For each *Task Condition*, both models estimated significantly

238 smaller peak  $F_C$  when using a BSE vs. the control condition. Depending on the specific *Task Condition*,  
 239 such reductions were estimated to be 10-14% in AMS and 14-21% in OpenSim.

240



241

242 Figure 5. *Task Condition*  $\times$  *Intervention*  $\times$  *Model* interaction effect on estimated peak (95<sup>th</sup> percentile)  
 243 compressive forces ( $F_C$ ) at L4/L5 as estimated using the AnyBody Modeling System (AMS) and  
 244 OpenSim.

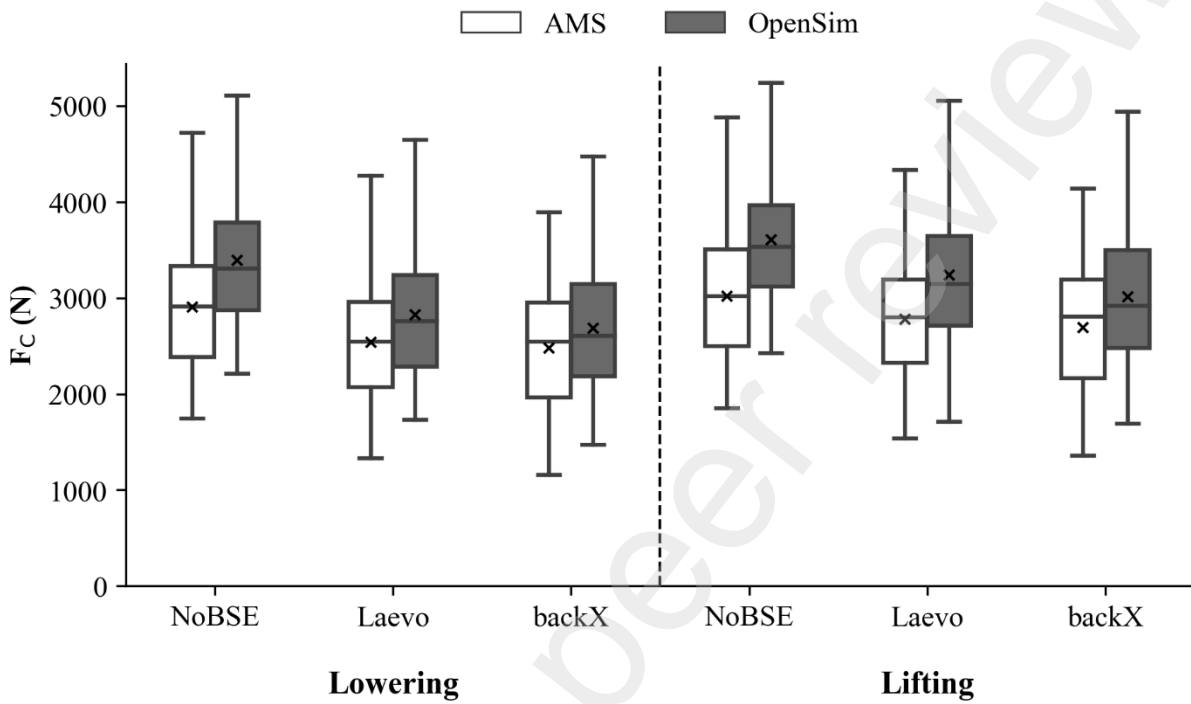
245

246 There was a significant interaction effect of *Intervention*  $\times$  *Movement Phase*  $\times$  *Model* on peak  $F_C$ . Simple  
 247 effects analysis indicated a significant interaction effect of *Intervention*  $\times$  *Model* in both the lowering and  
 248 lifting phases. Similarly, a significant *Movement Phase*  $\times$  *Model* interaction effect was observed for all  
 249 *Intervention* levels. Reductions in peak  $F_C$  estimated with BSE use were more pronounced during  
 250 lowering tasks (Figure 6). BSE use was estimated to decrease peak  $F_C$  by 13–16% in AMS and 18–22%

251 in OpenSim during lowering tasks, compared to 9–12% in AMS and 11–17% in OpenSim during lifting

252 tasks.

253



254

255 Figure 6. *Intervention × Movement Phase × Model* interaction effect on peak (95<sup>th</sup> percentile)

256

compressive forces ( $F_C$ ) at L4/L5.

257

### 258 3.3 Peak anteroposterior shear forces ( $F_{AP}$ ) at L4/L5

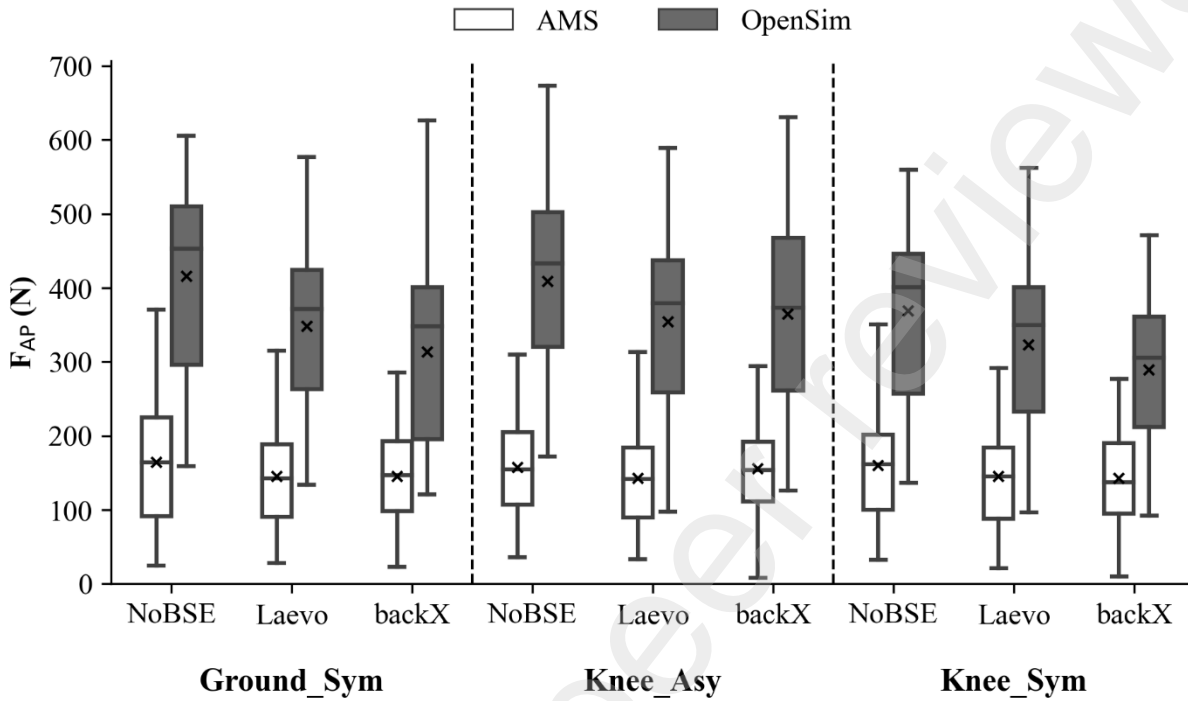
259 There was a significant effect of *Intervention × Task Condition × Model* on peak  $F_{AP}$ . Simple effects

260 analysis revealed significant *Intervention × Model* and *Task Condition × Model* interaction effects for all

261 levels of *Task Condition* and *Intervention*, respectively. Specifically, OpenSim estimated significantly

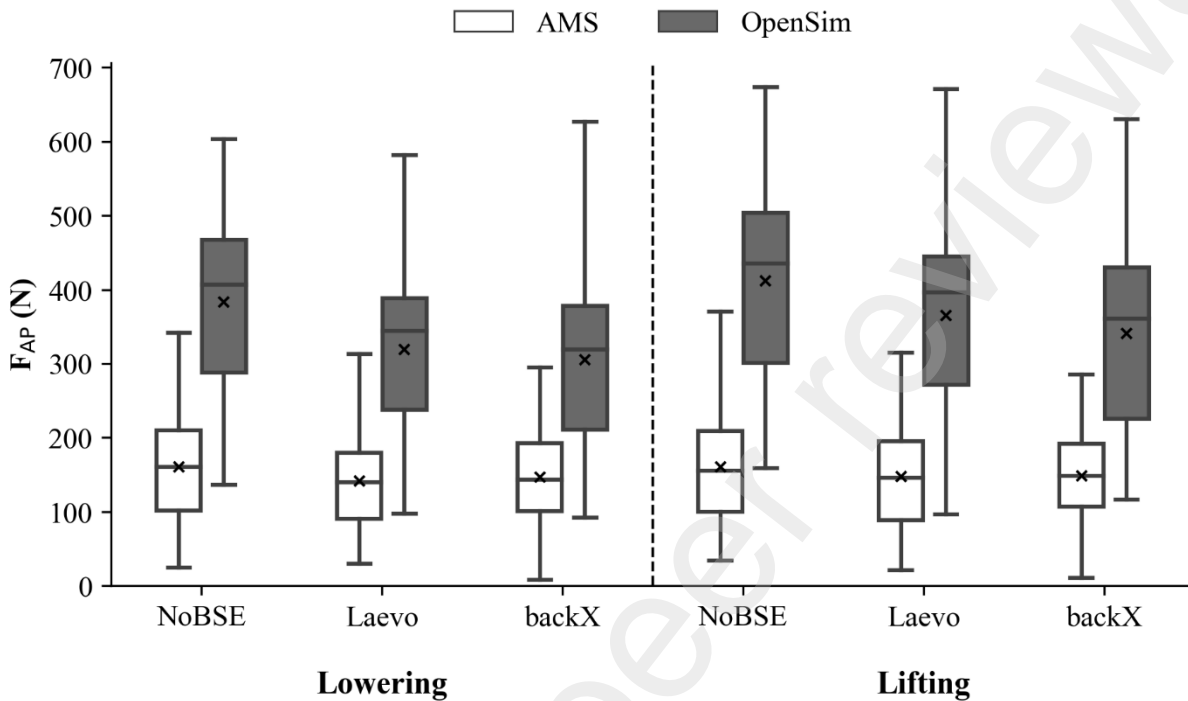
262 larger peak  $F_{AP}$  values than AMS across all conditions (by 119–173%). For all *Task Conditions*, BSE use

263 was estimated to significantly reduce peak  $F_{AP}$  values vs. the control condition. Such reductions were by  
 264 8-14% in AMS and 14-25% in OpenSim, depending on the specific *Task Condition* (Figure 7).



265  
 266 Figure 7. *Task Condition* × *Intervention* × *Model* interaction effect on peak (95<sup>th</sup> percentile)  
 267 anteroposterior shear forces ( $F_{AP}$ ) values at L4/L5.  
 268  
 269 We also found a significant interaction effect of *Intervention* × *Movement Phase* × *Model* on peak  $F_{AP}$ .  
 270 There were significant simple interaction effects of *Movement Phase* × *Model* for all levels of  
 271 *Intervention*. For both lowering and lifting, there was a significant interaction effect of *Intervention* ×  
 272 *Model*. BSE use was estimated to significantly reduce  $F_{AP}$  in AMS during lowering tasks, by 10–11%;

273 reductions in  $F_{AP}$  were more pronounced using OpenSim, ranging from 18–23%. During lifting tasks, the  
 274 reductions were smaller, being 9–10% in AMS and 12–19% in OpenSim (Figure 8).



275

276 Figure 8. *Intervention × Movement Phase × Model* interaction effect on peak (95<sup>th</sup> percentile)  
 277 anteroposterior shear forces ( $F_{AP}$ ) values at L4/L5.

278

### 279 3.4 Associations between model estimations ( $r$ )

280 For  $F_C$ , there were strong, positive, linear relationships between AMS and OpenSim estimations, with the  
 281 mean  $r$  for  $>0.95$  in all *Task Condition* (Figure A8, supplementary materials). In contrast,  $r$  values for  $F_{AP}$   
 282 indicated varied relationships across conditions (Figure 8). Weak positive linear relationships were  
 283 observed in the *Ground\_Sym* and *Knee\_Sym* conditions, except during the lifting phase when using  
 284 *backX*. Of note, moderate-strong *negative* linear relationships were observed in *Knee\_Asym*, regardless  
 285 of *Intervention* levels.

286

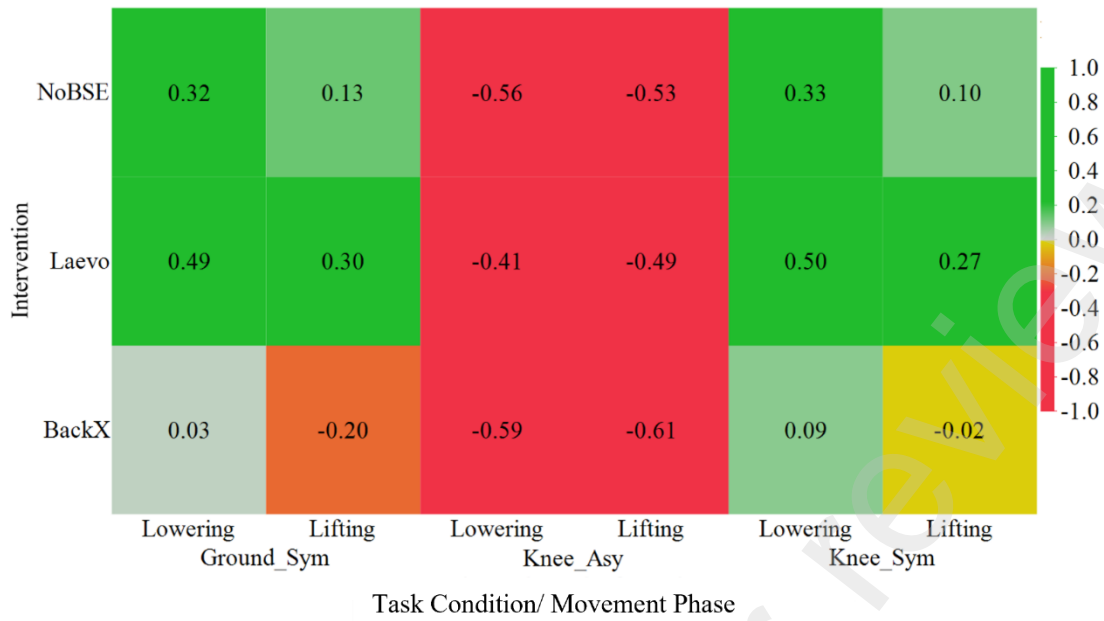


Figure 9. Heatmap of Pearson Correlation Coefficient ( $r$ ) values for  $F_{AP}$  times series as estimated by AnyBody (AMS) and OpenSim, across *Task Conditions*, *Interventions*, and *Movement Phases*.

#### 4. Discussion

We assessed spine loading estimates obtained from musculoskeletal models using AnyBody and OpenSim during repetitive lifting and lowering tasks, both with and without the use of BSEs. Both modeling tools estimated decreases in spine loading with the use of either of two BSEs compared to the control condition. This finding aligns with previous studies that reported 10–20% reductions in  $F_C$  and  $F_{AP}$  forces with BSE use (Koopman, Kingma, et al., 2020; Koopman, Näf, et al., 2020; Madinei & Nussbaum, 2023; Schmalz et al., 2022). However, we found that the magnitude of these reductions was larger using OpenSim (Figures 5–8). Associations between  $F_C$  time series obtained from the two tools in each experimental condition were generally strong and positive in all experimental conditions ( $r$  values  $>0.95$ ). But these associations were both weaker and more variable (ranging from positive to negative) for  $F_{AP}$ . Our findings suggest that, overall, while both modeling tools can assess the effects of BSEs, differences in their outputs should be considered carefully prior to practical decision-making.

303

304 We believe there are multiple factors that might account for the larger reductions in IJFs with BSE use  
305 when estimated using OpenSim vs. AMS (Figures 5– 8). One such factor is how a BSE was modeled in  
306 these tools to apply human-exoskeleton interaction forces—derived from BSE supportive torques—and  
307 other modeling specifics. When individuals bend forward while wearing a BSE, the chest frame could  
308 move cranially to some extent, shifting the application point of interaction forces further from the lower  
309 back. This movement can be accounted for in OpenSim by defining the interaction forces to originate  
310 from the chest frame, but a similar approach cannot be implemented easily in AMS. Thus, we applied  
311 interaction forces in AMS at a fixed location, as in Eskandari et al. (2025). The resultant external torque  
312 about L4/L5 during trunk flexion in AMS might be smaller than that in OpenSim for the same calculated  
313 interaction force in extreme postures, contributing to the observed differences in IJF values. Despite these  
314 differences,  $F_C$  time series from AMS and OpenSim had strong, positive associations across all lifting  
315 conditions (Figure A8).

316

317 In contrast,  $F_{AP}$  time series showed much weaker associations between ASM and OpenSim, particularly in  
318 the Knee-Asy and Ground-Sym conditions (Figures 3, 4, and 9). We suspect that an important contributor  
319 to these discrepancies is differences in ligament modeling. The Gait-full-body model in AMS uses  
320 nonlinear passive elastic elements to represent ligaments (Chazal et al., 1985). In contrast, the enhanced  
321 FATLS model in OpenSim employs bushing elements, a simplified stiffness model that estimates  
322 ligament contributions as passive torques in the spine (Akhavanfar et al., 2024). Other differences in spine  
323 modeling assumptions may have also contributed to divergences in model estimates, including  
324 optimization strategies (Wang et al., 2022), spine structure representations (Bruno et al., 2017), spine  
325 structure modeling (Ghezelbash et al., 2018; Ignasiak et al., 2016), and algorithms for creating subject-  
326 specific models (Ghezelbash et al., 2016). A detailed analysis of the underlying sources of differences in  
327 the estimated IJFs was beyond our current scope, but we hope to complete such analyses in follow-up  
328 work.

329

Several limitations in the current work were noted earlier by Madinei and Nussbaum (2023), including neglecting the effects of BSE mass and any relative displacements between the BSE and human hip joints, as well as errors related to reconstructing motion data from the inertial motion capture system. Some additional limitations should be acknowledged. First, our virtual BSE representation was simplified by excluding inertial properties and soft materials (e.g., straps and belts). The human-exoskeleton interface was also simplified by using kinematic constraints (Ferrati et al., 2013; Madinei & Nussbaum, 2023; Zhou et al., 2017), rather than using more complex and potentially more realistic approaches such as force-generating elements (Fournier et al., 2018; Tröster et al., 2020) or rigid-body contact force modeling (Chander et al., 2022; Cho et al., 2012). While these methods could offer greater accuracy, they are also quite computationally expensive, particularly for large-scale simulations. Future research should focus on how to best balance model complexity with computational efficiency for BSE (and other exoskeleton) modeling. Second, although there is evidence that estimates from OpenSim and AMS align with *in vivo* data (Alemi et al., 2023; Bassani et al., 2017; Yan et al., 2024), the fidelity and applicability of these models to activities involving BSEs remain unclear (e.g., due to simplifications of the human-exoskeleton interface noted above). We thus encourage future comparisons between modeling tools across various exoskeleton types and manual tasks.

In summary, we found that both AMS and OpenSim estimate that BSE use significantly reduced spine loading during symmetric and asymmetric lifting tasks. Both models indicated that BSE use significantly reduces peak  $F_C$  and  $F_{AP}$ , underscoring the potential of musculoskeletal modeling in assessing BSEs as an ergonomic intervention. However, OpenSim consistently estimated larger overall IJF values and larger reductions in IJFs when using a BSE, particularly for  $F_{AP}$ . Strong positive associations were found in  $F_C$  estimated between the two models, whereas  $F_{AP}$  estimates showed substantially weaker associations, particularly in extreme postures. These discrepancies may have arisen from differences in how the models account for passive structures and force redistribution during lifting motions. Future research should focus on refining human-exoskeleton interaction models, incorporating more realistic representations of passive

356 tissues, and validating findings against *in vivo* data to improve the accuracy and applicability of  
357 musculoskeletal simulations for exoskeletons as an ergonomic intervention.

358

359 **6. Acknowledgment**

360 This study was supported by Grant # 2128926 from the National Science Foundation (NSF). The sponsor  
361 was not involved in data analysis, interpretation, or the decision to publish. The current contents are  
362 solely the responsibility of the authors and do not necessarily reflect the views of NSF.

363

364 **7. Declaration of generative AI and AI-assisted technologies in the writing process**

365 *During the preparation of this work, we used ChatGPT to refine some sentences and improve the  
366 clarity of the text. After using this tool/service, we reviewed and edited the content as needed,  
367 and we take full responsibility for the content of this publication.*

368 **References**

- 369 Akhavanfar, M., Mir-Orefice, A., Uchida, T. K., & Graham, R. B. (2024). An Enhanced Spine Model  
 370 Validated for Simulating Dynamic Lifting Tasks in OpenSim. *Annals of Biomedical Engineering*,  
 371 52(2), 259-269. <https://doi.org/10.1007/s10439-023-03368-x>
- 372 Alemi, M. M., Banks, J. J., Lynch, A. C., Allaire, B. T., Bouxsein, M. L., & Anderson, D. E. (2023). EMG  
 373 validation of a subject-specific thoracolumbar spine musculoskeletal model during dynamic  
 374 activities in older adults. *Annals of Biomedical Engineering*, 51(10), 2313-2322.  
 375 <https://doi.org/10.1007/s10439-023-03273-3>
- 376 Alemi, M. M., Madinei, S., Kim, S., Srinivasan, D., & Nussbaum, M. A. (2020). Effects of two passive  
 377 back-support exoskeletons on muscle activity, energy expenditure, and subjective assessments  
 378 during repetitive lifting. *Human factors*, 62(3), 458-474.  
 379 <https://doi.org/10.1177/0018720819897669>
- 380 Ali, A., Fontanari, V., Schmoelz, W., & Agrawal, S. K. (2021). Systematic review of back-support  
 381 exoskeletons and soft robotic suits. *Frontiers in bioengineering and biotechnology*, 9, 765257.  
 382 <https://doi.org/10.3389/fbioe.2021.765257>
- 383 Andersen, M. S., Damsgaard, M., & Rasmussen, J. (2009). Kinematic analysis of over-determinate  
 384 biomechanical systems. *Computer methods in biomechanics and biomedical engineering*, 12(4),  
 385 371-384. <https://doi.org/10.1080/10255840802459412>
- 386 Banks, J. J., Quirk, D. A., Chung, J., Cherin, J. M., Walsh, C. J., & Anderson, D. E. (2024). The effect of a  
 387 soft active back support exosuit on trunk motion and thoracolumbar spine loading during squat and  
 388 stoop lifts. *Ergonomics*, 1-14. <https://doi.org/10.1080/00140139.2024.2320355>
- 389 Bassani, T., Stucovitz, E., Qian, Z., Briguglio, M., & Galbusera, F. (2017). Validation of the AnyBody full  
 390 body musculoskeletal model in computing lumbar spine loads at L4L5 level. *Journal of  
 391 Biomechanics*, 58, 89-96. <https://doi.org/10.1080/10255840802459412>
- 392 Bosch, T., van Eck, J., Knitel, K., & de Looze, M. (2016). The effects of a passive exoskeleton on muscle  
 393 activity, discomfort and endurance time in forward bending work. *Applied ergonomics*, 54, 212-  
 394 217. <https://doi.org/10.1016/j.apergo.2015.12.003>
- 395 Bruno, A. G., Bouxsein, M. L., & Anderson, D. E. (2015). Development and validation of a musculoskeletal  
 396 model of the fully articulated thoracolumbar spine and rib cage. *Journal of biomechanical  
 397 engineering*, 137(8), 081003. <https://doi.org/10.1115/1.4030408>
- 398 Bruno, A. G., Burkhardt, K., Allaire, B., Anderson, D. E., & Bouxsein, M. L. (2017). Spinal loading patterns  
 399 from biomechanical modeling explain the high incidence of vertebral fractures in the  
 400 thoracolumbar region. *Journal of Bone and Mineral Research*, 32(6), 1282-1290.  
 401 <https://doi.org/10.1002/jbmr.3113>
- 402 Chander, D. S., Böhme, M., Andersen, M. S., Rasmussen, J., Zentner, J., & Cavatorta, M. P. (2022). A  
 403 comparison of different methods for modelling the physical human-exoskeleton interface.  
 404 *International journal of human factors modelling and simulation*, 7(3-4), 204-230.  
 405 <https://doi.org/10.1504/IJHFMS.2022.124310>
- 406 Chazal, J., Tangy, A., Bourges, M., Gaurel, G., Escande, G., Guillot, M., & Vanneuville, G. (1985).  
 407 Biomechanical properties of spinal ligaments and a histological study of the supraspinal ligament  
 408 in traction. *Journal of Biomechanics*, 18(3), 167-176. [https://doi.org/10.1016/0021-9290\(85\)90202-7](https://doi.org/10.1016/0021-9290(85)90202-7)
- 409 Cho, K., Kim, Y., Yi, D., Jung, M., & Lee, K. (2012). Analysis and evaluation of a combined human-  
 410 exoskeleton model under two different constraints condition. *Proceedings of the International  
 411 Summit on Human Simulation*, 5, 23-25.
- 412 Damsgaard, M., Rasmussen, J., Christensen, S. T., Surma, E., & De Zee, M. (2006). Analysis of  
 413 musculoskeletal systems in the AnyBody Modeling System. *Simulation Modelling Practice and  
 414 Theory*, 14(8), 1100-1111. <https://doi.org/10.1016/j.simpat.2006.09.001>

- 416 de Looze, M. P., Bosch, T., Krause, F., Stadler, K. S., & O'sullivan, L. W. (2016). Exoskeletons for  
 417 industrial application and their potential effects on physical work load. *Ergonomics*, 59(5), 671-  
 418 681. <https://doi.org/10.1080/00140139.2015.1081988>
- 419 Delp, S. L., Anderson, F. C., Arnold, A. S., Loan, P., Habib, A., John, C. T., Guendelman, E., & Thelen,  
 420 D. G. (2007). OpenSim: open-source software to create and analyze dynamic simulations of  
 421 movement. *IEEE Transactions on Biomedical Engineering*, 54(11), 1940-1950.  
 422 <https://doi.org/10.1109/TBME.2007.901024>
- 423 Eskandari, A. H., Ghezelbash, F., Shirazi-Adl, A., Arjmand, N., & Larivière, C. (2025). Effect of a back-  
 424 support exoskeleton on internal forces and lumbar spine stability during low load lifting task.  
 425 *Applied ergonomics*, 123, 104407. <https://doi.org/10.1016/j.apergo.2024.104407>
- 426 Ferrati, F., Bortoletto, R., & Pagello, E. (2013). Virtual modelling of a real exoskeleton constrained to a  
 427 human musculoskeletal model. *Biomimetic and Biohybrid Systems: Second International  
 428 Conference, Living Machines 2013, London, UK, July 29–August 2, 2013. Proceedings* 2, 96-107.  
 429 [https://doi.org/10.1007/978-3-642-39802-5\\_9](https://doi.org/10.1007/978-3-642-39802-5_9)
- 430 Fournier, B. N., Lemaire, E. D., Smith, A. J., & Doumit, M. (2018). Modeling and simulation of a lower  
 431 extremity powered exoskeleton. *IEEE transactions on neural systems and rehabilitation  
 432 engineering*, 26(8), 1596-1603. <https://doi.org/10.1109/TNSRE.2018.2854605>
- 433 Ghezelbash, F., Eskandari, A., Shirazi-Adl, A., Arjmand, N., El-Ouaaid, Z., & Plamondon, A. (2018).  
 434 Effects of motion segment simulation and joint positioning on spinal loads in trunk musculoskeletal  
 435 models. *Journal of Biomechanics*, 70, 149-156. <https://doi.org/10.1016/j.jbiomech.2017.07.014>
- 436 Ghezelbash, F., Shirazi-Adl, A., Arjmand, N., El-Ouaaid, Z., & Plamondon, A. (2016). Subject-specific  
 437 biomechanics of trunk: musculoskeletal scaling, internal loads and intradiscal pressure estimation.  
 438 *Biomechanics and modeling in mechanobiology*, 15, 1699-1712. <https://doi.org/10.1007/s10237-016-0792-3>
- 439 Ghezelbash, F., Shirazi-Adl, A., Plamondon, A., & Arjmand, N. (2020). Comparison of different lifting  
 440 analysis tools in estimating lower spinal loads—Evaluation of NIOSH criterion. *Journal of  
 441 Biomechanics*, 112, 110024. <https://doi.org/10.1016/j.jbiomech.2020.110024>
- 442 Ignasiak, D., Ferguson, S. J., & Arjmand, N. (2016). A rigid thorax assumption affects model loading  
 443 predictions at the upper but not lower lumbar levels. *Journal of Biomechanics*, 49(13), 3074-3078.  
 444 <https://doi.org/10.1016/j.jbiomech.2016.07.006>
- 445 Karatsidis, A., Jung, M., Schepers, H. M., Bellusci, G., de Zee, M., Veltink, P. H., & Andersen, M. S.  
 446 (2019). Musculoskeletal model-based inverse dynamic analysis under ambulatory conditions using  
 447 inertial motion capture. *Medical Engineering & Physics*, 65, 68-77.  
 448 <https://doi.org/10.1016/j.medengphy.2018.12.021>
- 449 Kazerooni, H. (2008). A review of the exoskeleton and human augmentation technology. *Dynamic Systems  
 450 and Control Conference*, 43352, 1539-1547. <https://doi.org/10.1115/DSCC2008-2407>
- 451 Kermavnar, T., de Vries, A. W., de Looze, M. P., & O'Sullivan, L. W. (2021). Effects of industrial back-  
 452 support exoskeletons on body loading and user experience: An updated systematic review.  
 453 *Ergonomics*, 64(6), 685-711. <https://doi.org/10.1080/00140139.2020.1870162>
- 454 Kim, Y., Jung, Y., Choi, W., Lee, K., & Koo, S. (2018). Similarities and differences between  
 455 musculoskeletal simulations of OpenSim and AnyBody modeling system. *Journal of Mechanical  
 456 Science and Technology*, 32, 6037-6044. <https://doi.org/10.1007/s12206-018-1154-0>
- 457 Koopman, A. S., Kingma, I., de Looze, M. P., & van Dieën, J. H. (2020). Effects of a passive back  
 458 exoskeleton on the mechanical loading of the low-back during symmetric lifting. *Journal of  
 459 Biomechanics*, 102, 109486. <https://doi.org/10.1016/j.jbiomech.2019.109486>
- 460 Koopman, A. S., Näf, M., Baltrusch, S. J., Kingma, I., Rodriguez-Guerrero, C., Babić, J., de Looze, M. P.,  
 461 & van Dieën, J. H. (2020). Biomechanical evaluation of a new passive back support exoskeleton.  
 462 *Journal of Biomechanics*, 105, 109795. <https://doi.org/10.1016/j.jbiomech.2020.109795>
- 463 Lamers, E. P., Yang, A. J., & Zelik, K. E. (2017). Feasibility of a biomechanically-assistive garment to  
 464 reduce low back loading during leaning and lifting. *IEEE Transactions on Biomedical Engineering*,  
 465 65(8), 1674-1680. <https://doi.org/10.1109/TBME.2017.2761455>

- 467 Lee, H., Kim, W., Han, J., & Han, C. (2012). The technical trend of the exoskeleton robot system for human  
 468 power assistance. *International Journal of Precision Engineering and Manufacturing*, 13, 1491-  
 469 1497. <https://doi.org/10.1007/s12541-012-0197-x>
- 470 Lund, M. E., Rasmussen, J., & Andersen, M. S. (2019). AnyPyTools: A Python package for reproducible  
 471 research with the AnyBody Modeling System. *The Journal of Open Source Software*, 4(33), 1108.  
 472 <https://doi.org/10.21105/joss.01108>
- 473 Ma, T., Zhang, Y., Choi, S. D., & Xiong, S. (2023). Modelling for design and evaluation of industrial  
 474 exoskeletons: A systematic review. *Applied ergonomics*, 113, 104100.  
 475 <https://doi.org/10.1016/j.apergo.2023.104100>
- 476 Madinei, S., Alemi, M. M., Kim, S., Srinivasan, D., & Nussbaum, M. A. (2020). Biomechanical assessment  
 477 of two back-support exoskeletons in symmetric and asymmetric repetitive lifting with moderate  
 478 postural demands. *Applied ergonomics*, 88, 103156. <https://doi.org/10.1016/j.apergo.2020.103156>
- 479 Madinei, S., & Nussbaum, M. A. (2023). Estimating lumbar spine loading when using back-support  
 480 exoskeletons in lifting tasks. *Journal of Biomechanics*, 147, 111439.  
 481 <https://doi.org/10.1016/j.jbiomech.2023.111439>
- 482 Rasmussen, J., de Zee, M., Damsgaard, M., Christensen, S. T., Marek, C., & Siebertz, K. (2005). A general  
 483 method for scaling musculo-skeletal models. *2005 international symposium on computer  
 484 simulation in biomechanics*.
- 485 Schmalz, T., Colienne, A., Bywater, E., Fritzsche, L., Gärtner, C., Bellmann, M., Reimer, S., & Ernst, M.  
 486 (2022). A passive back-support exoskeleton for manual materials handling: reduction of low back  
 487 loading and metabolic effort during repetitive lifting. *IIEE transactions on occupational  
 488 ergonomics and human factors*, 10(1), 7-20. <https://doi.org/10.1080/24725838.2021.2005720>
- 489 Tröster, M., Wagner, D., Müller-Graf, F., Maufroy, C., Schneider, U., & Bauernhansl, T. (2020).  
 490 Biomechanical model-based development of an active occupational upper-limb exoskeleton to  
 491 support healthcare workers in the surgery waiting room. *International Journal of Environmental  
 492 Research and Public Health*, 17(14), 5140. <https://doi.org/10.3390/ijerph17145140>
- 493 Wang, W., Wang, D., & Li, G. (2022). Towards improving the accuracy of musculoskeletal simulation of  
 494 dynamic three-dimensional spine rotations with optimizing model and algorithm. *Medical  
 495 Engineering & Physics*, 110, 103916. <https://doi.org/10.1016/j.medengphy.2022.103916>
- 496 Waters, T. R., Putz-Anderson, V., Garg, A., & Fine, L. J. (1993). Revised NIOSH equation for the design  
 497 and evaluation of manual lifting tasks. *Ergonomics*, 36(7), 749-776.  
 498 <https://doi.org/10.1080/00140139308967940>
- 499 Wechsler, I., Wolf, A., Fleischmann, S., Waibel, J., Molz, C., Scherb, D., Shanbhag, J., Franz, M.,  
 500 Wartzack, S., & Miehling, J. (2023). Method for using IMU-based experimental motion data in  
 501 BVH format for musculoskeletal simulations via OpenSim. *Sensors*, 23(12), 5423.  
 502 <https://doi.org/10.3390/s23125423>
- 503 Wu, G., Van der Helm, F. C., Veeger, H. D., Makhsoos, M., Van Roy, P., Anglin, C., Nagels, J., Karduna,  
 504 A. R., McQuade, K., & Wang, X. (2005). ISB recommendation on definitions of joint coordinate  
 505 systems of various joints for the reporting of human joint motion—Part II: shoulder, elbow, wrist  
 506 and hand. *Journal of Biomechanics*, 38(5), 981-992.  
 507 <https://doi.org/10.1016/j.jbiomech.2004.05.042>
- 508 Yan, C., Banks, J. J., Allaire, B. T., Quirk, D. A., Chung, J., Walsh, C. J., & Anderson, D. E. (2024).  
 509 Musculoskeletal models determine the effect of a soft active exosuit on muscle activations and  
 510 forces during lifting and lowering tasks. *Journal of Biomechanics*, 176, 112322.  
 511 <https://doi.org/10.1016/j.jbiomech.2024.112322>
- 512 Zhou, L., Li, Y., & Bai, S. (2017). A human-centered design optimization approach for robotic exoskeletons  
 513 through biomechanical simulation. *Robotics and Autonomous Systems*, 91, 337-347.  
 514 <https://doi.org/10.1016/j.robot.2016.12.012>
- 515

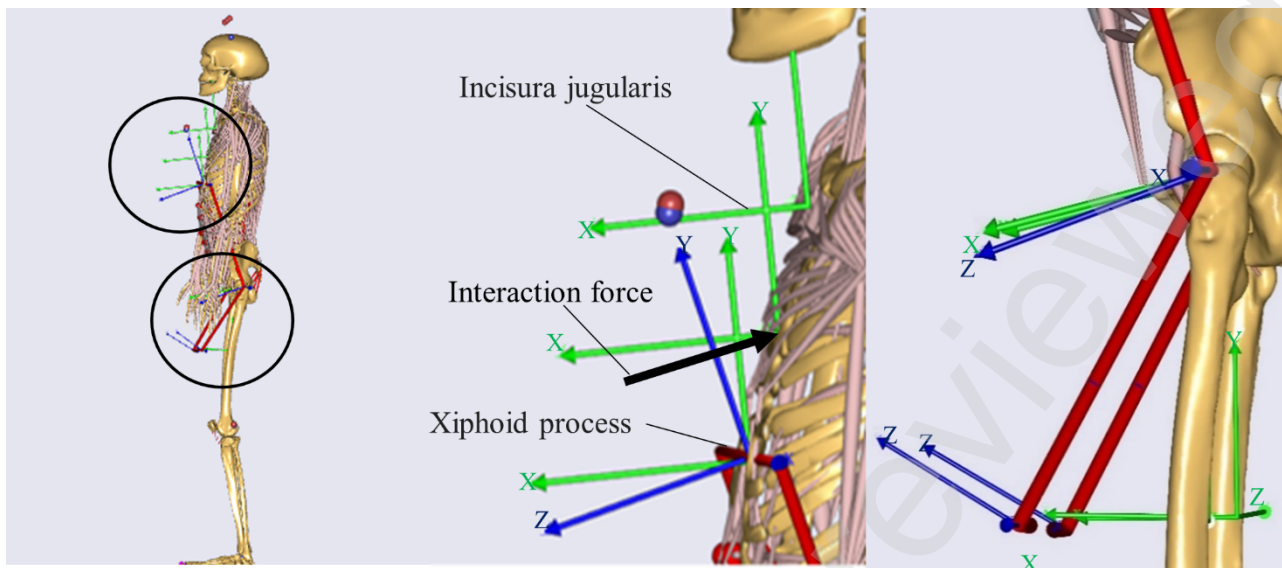


Figure 1. Illustrations of a virtual BSE representation in the AnyBody Modeling System (AMS). The middle and right figures show zoomed-in views of the coordinate systems for the BSE (blue) and the Gait-full-body model (green) at the torso and leg frames, respectively. The black arrow indicates the interaction force between the BSE and the Gait-full-body model, applied to a contact point on the chest (the origin of the body coordinate system in green) and aligned parallel to the normal axis (blue Z-axis) of the BSE torso plate (chest pad).

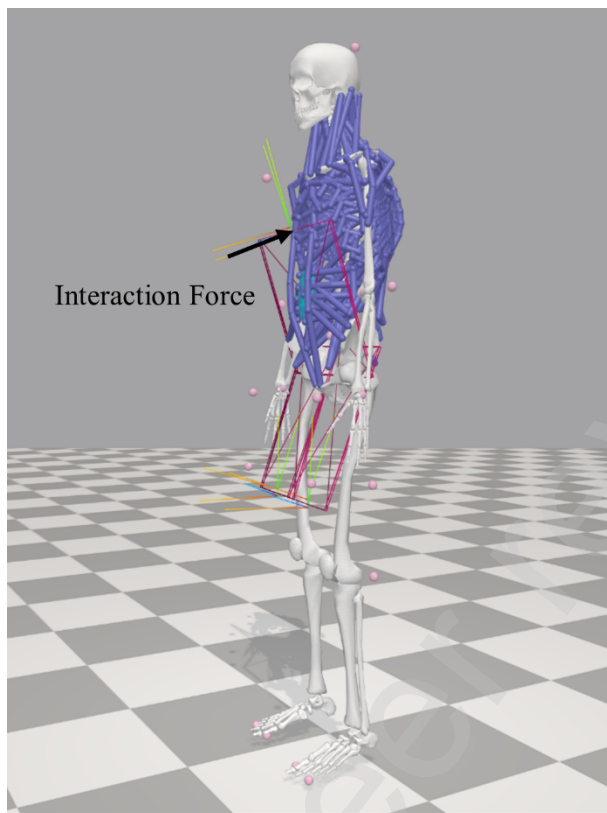


Figure 2. Illustration of the virtual BSE representation in OpenSim. The black arrow represents the interaction force between the BSE and the FATLS model, which is applied to the thorax. Pink balls represent VMs in the human model.

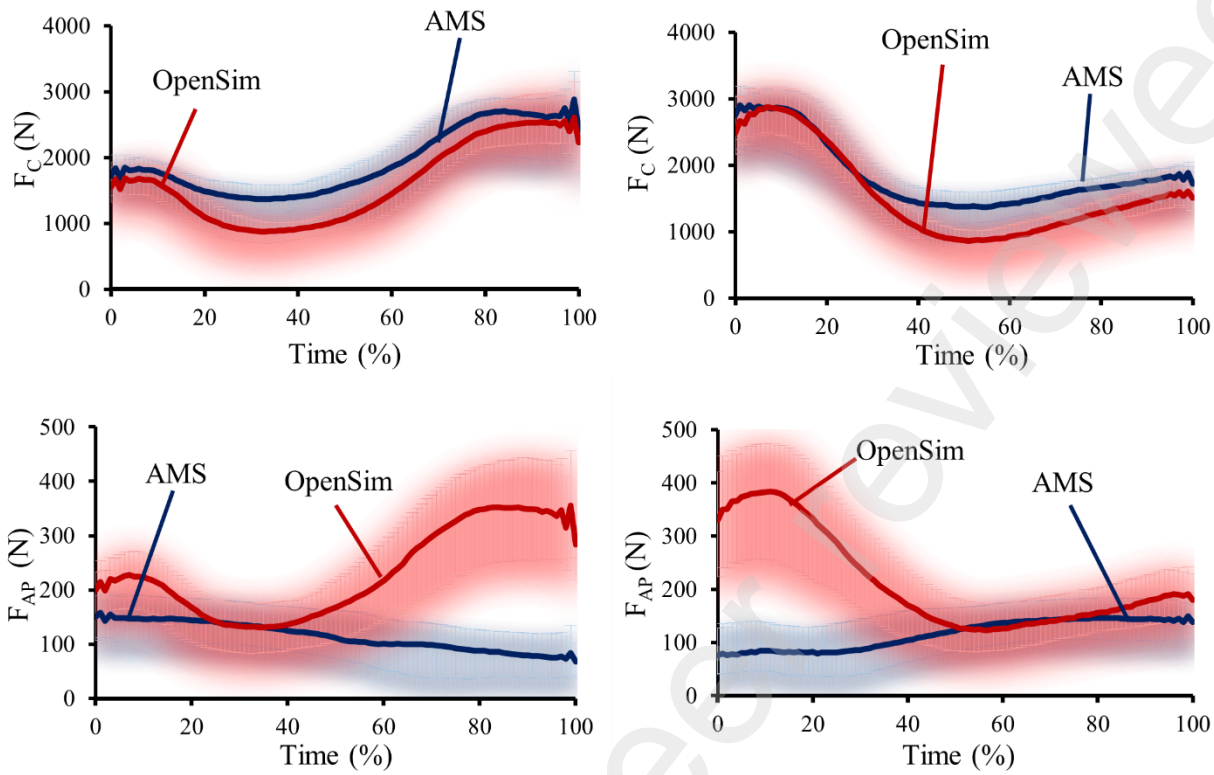


Figure 3. Example ensemble median plots of intervertebral joint forces at the L4/L5 intervertebral joint, comparing results from OpenSim and AnyBody (AMS) for the Knee\_Asy task when using backX. This condition was selected as it represents the “worst” condition, highlighting substantial differences in estimates of  $F_{AP}$ . **Top left:** Compression Forces ( $F_C$ ) during lowering. **Top right:**  $F_C$  during lifting.

**Bottom left:** Anteroposterior Shear Forces ( $F_{AP}$ ) during lowering. **Bottom right:**  $F_{AP}$  during lifting.

Shaded areas represent 25<sup>th</sup> and 75<sup>th</sup> percentile values.

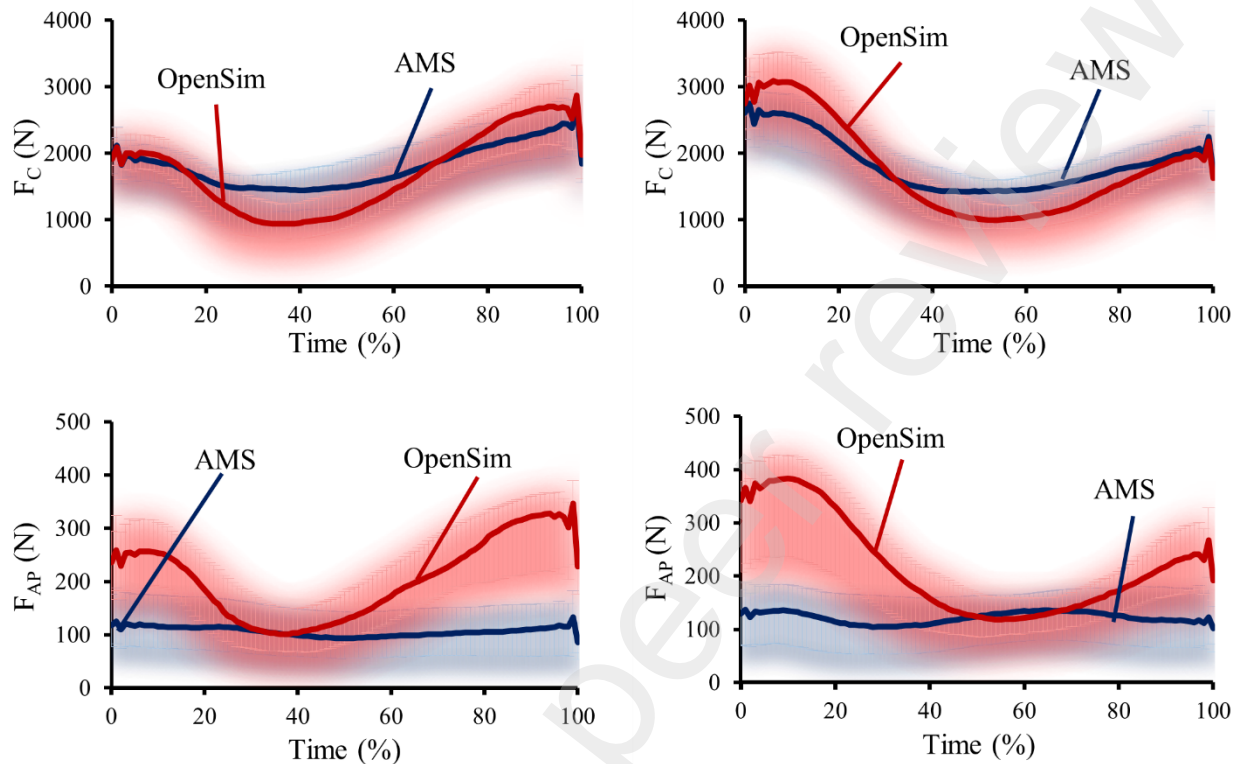


Figure 4. Example ensemble median plots of intervertebral joint forces at the L4/L5 intervertebral joint comparing results from OpenSim and AnyBody (AMS) for the Knee\_Sym task when using Laevo. This condition was selected as it represents the “best” condition, with similar trend for estimates of  $F_{AP}$ . **Top left:** Compression Forces ( $F_C$ ) during lowering. **Top right:**  $F_C$  during lifting. **Bottom left:**

**Bottom right:**  $F_{AP}$  during lifting. Shaded areas represent the 25<sup>th</sup> and 75<sup>th</sup> percentile values.

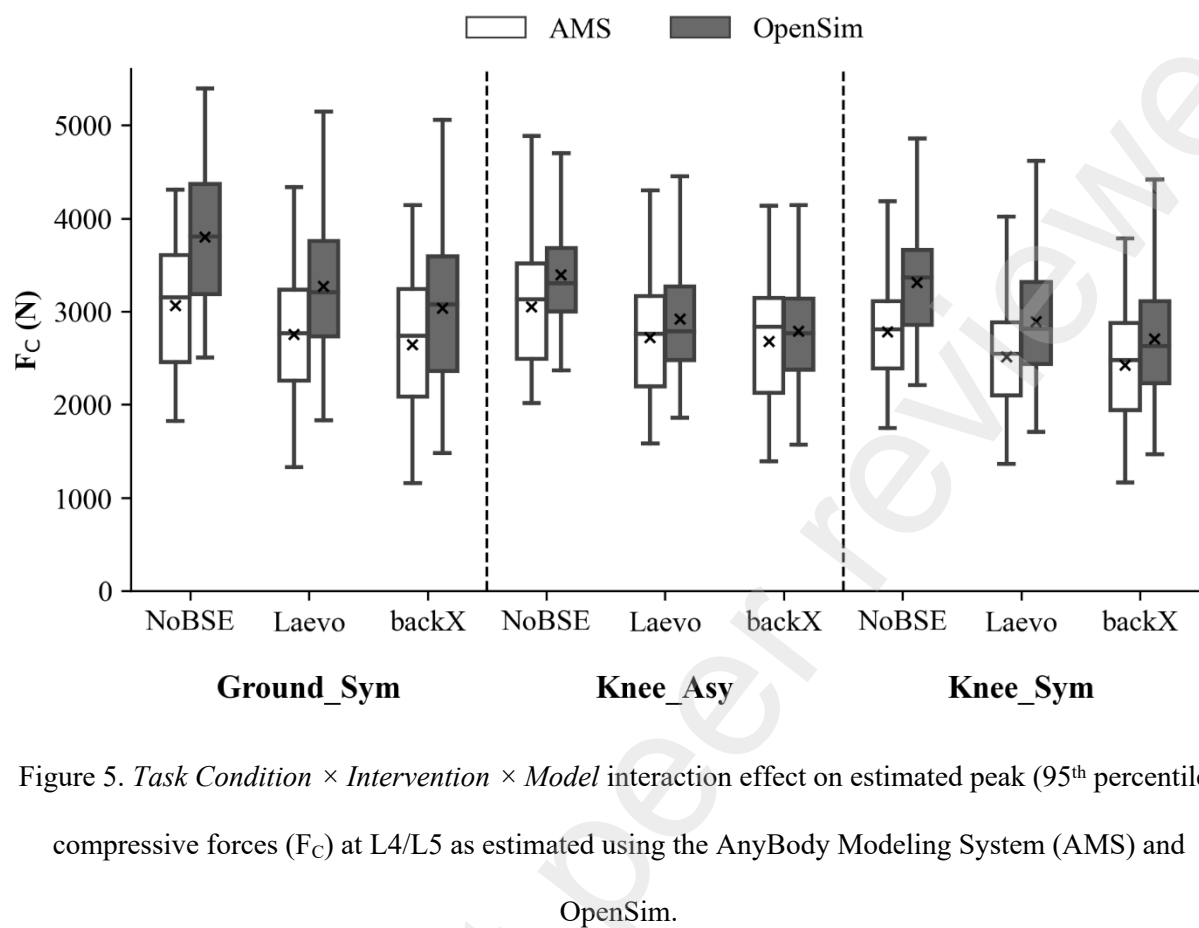


Figure 5. *Task Condition*  $\times$  *Intervention*  $\times$  *Model* interaction effect on estimated peak (95<sup>th</sup> percentile) compressive forces ( $F_C$ ) at L4/L5 as estimated using the AnyBody Modeling System (AMS) and OpenSim.

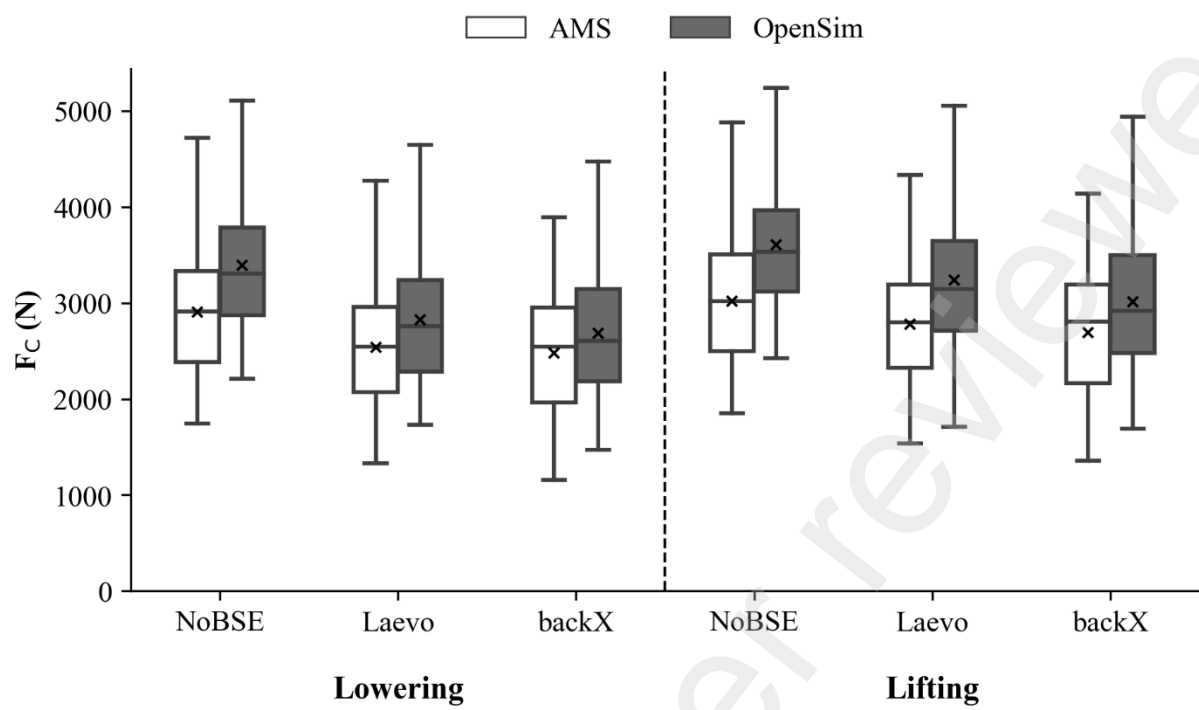


Figure 6. *Intervention*  $\times$  *Movement Phase*  $\times$  *Model* interaction effect on peak (95<sup>th</sup> percentile) compressive forces (F<sub>C</sub>) at L4/L5.

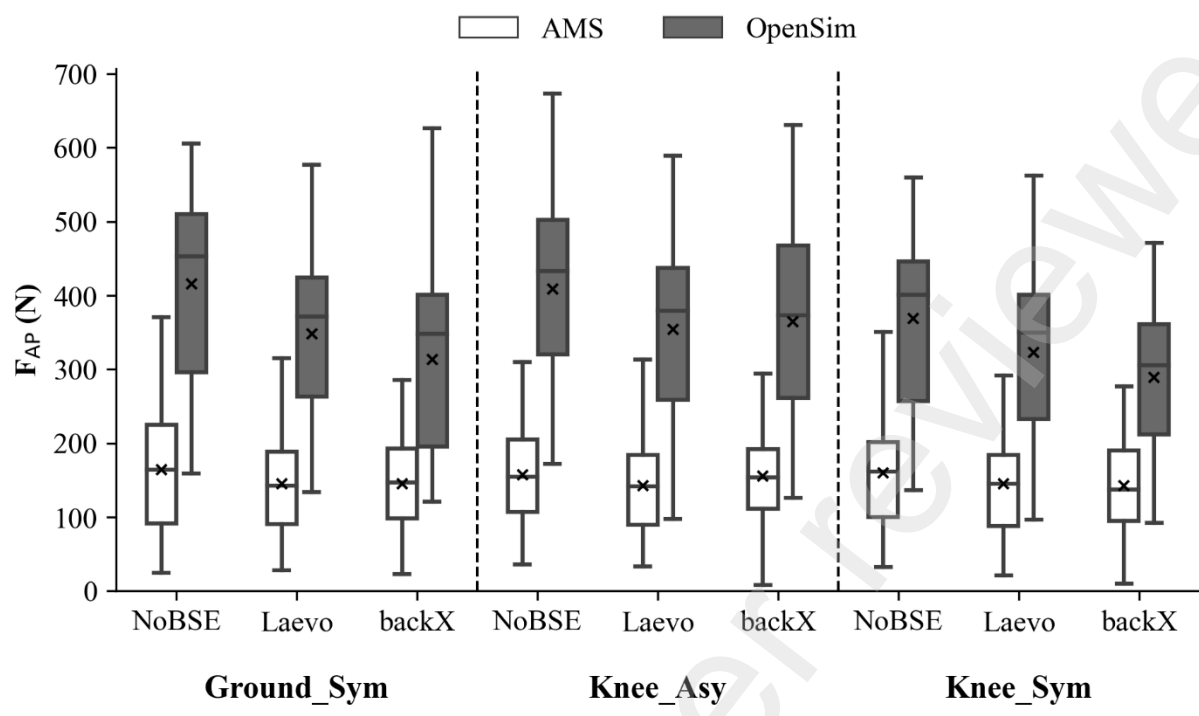


Figure 7. *Task Condition* × *Intervention* × *Model* interaction effect on peak (95<sup>th</sup> percentile) anteroposterior shear forces (F<sub>AP</sub>) values at L4/L5.

anteroposterior shear forces (F<sub>AP</sub>) values at L4/L5.

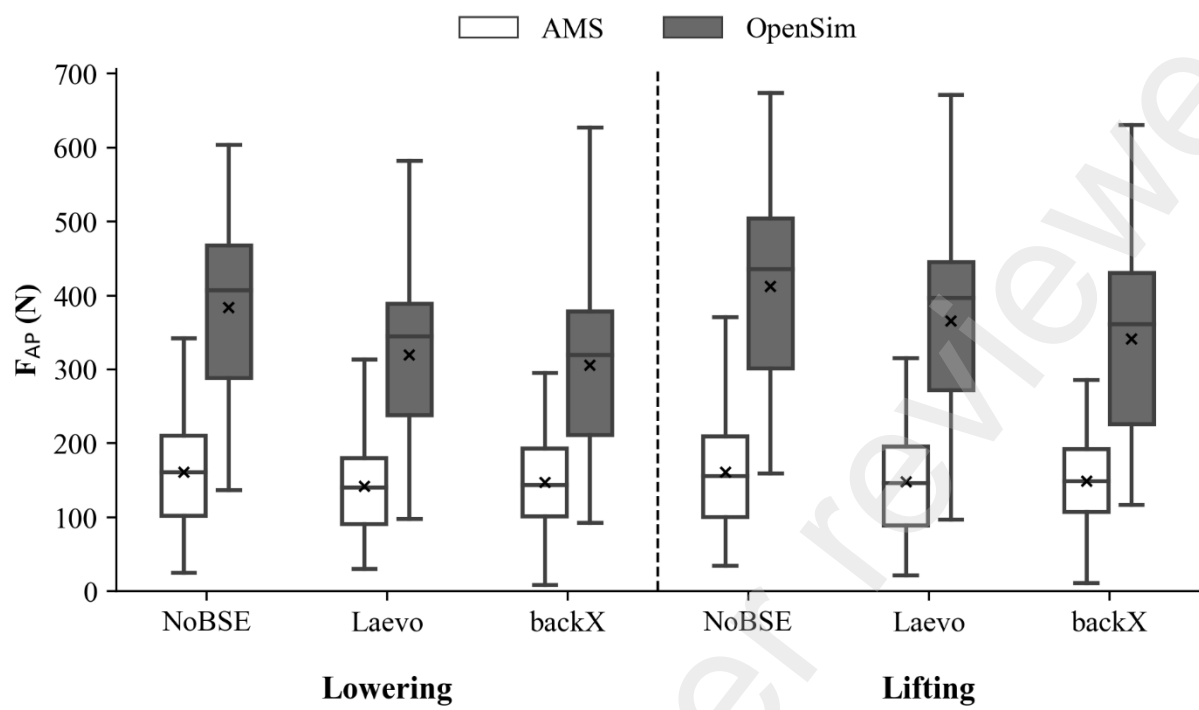


Figure 8. *Intervention*  $\times$  *Movement Phase*  $\times$  *Model* interaction effect on peak (95<sup>th</sup> percentile)

anteroposterior shear forces (F<sub>AP</sub>) values at L4/L5.

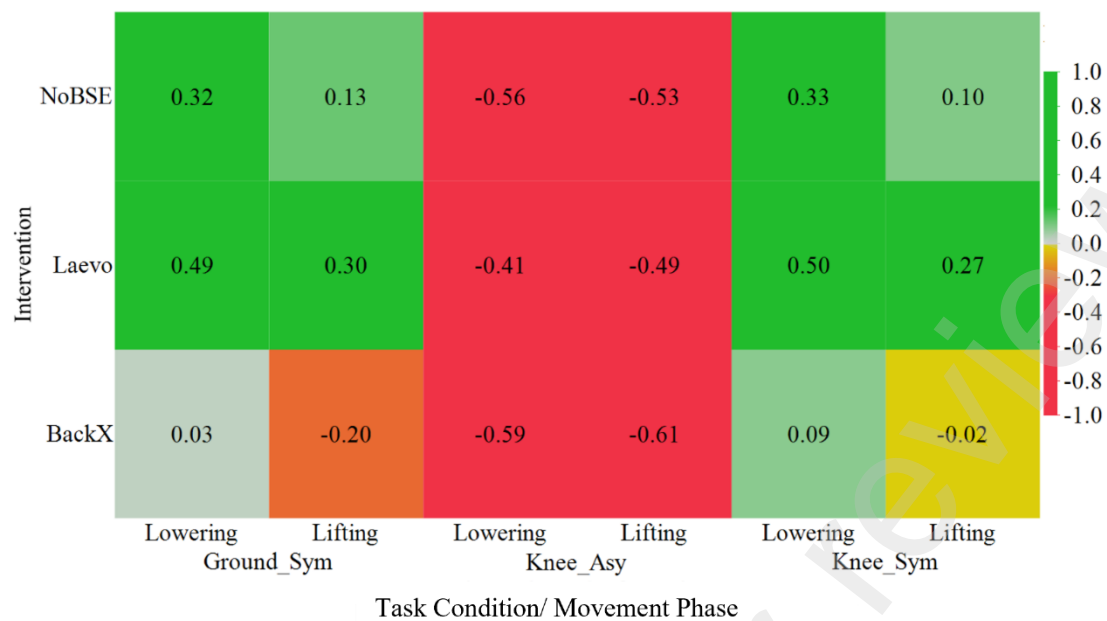


Figure 9. Heatmap of Pearson Correlation Coefficient ( $r$ ) values for  $F_{AP}$  times series as estimated by AnyBody (AMS) and OpenSim, across *Task Conditions*, *Interventions*, and *Movement Phases*.